Analytical study of pre-stall hydrofoil experimental data for a cyclorotor-based wave energy converter

Andrei Ermakov
Centre for Ocean Energy Research
Maynooth University
Maynooth, Ireland
andrei.ermakov@mu.ie

Florent Thiebaut
Ecole Centrale de Nantes
Nantes, France
florent.thiebaut@ec-nantes.fr

Grégory S. Payne
Ecole Centrale de Nantes
Nantes, France
gregory.payne@farwind-energy.com

John V. Ringwood
Centre for Ocean Energy Research
Maynooth University
Maynooth, Ireland
john.ringwood@mu.ie

***Abstract*—Cyclorotor-based wave energy converters (WECs), that utilise lift forces generated on hydrofoils due to their interaction with the wave-induced circular motion of water particles, have received recent attention from various researchers and organisations. Cyclorotor WECs have a number of appealing characteristics, including the potential for fast unidirectional rotation, simple power take-off, and relatively low wave loads by adjusting pitch angles, increasing survivability and capacity factor.**

The published analytical assessments of cyclorotor performance have shown that a cyclorotor achieves maximum performance in terms of wave cancellation, or mechanical shaft power generation, when its hydrofoils operate in the vicinity of the stall angle of attack. Such performance assessments are based on ideal lift and drag coefficient values obtained for aerofoils in aerodynamic tubes. In this study, we question the equivalence between aerofoils and hydrofoils in waves, in terms of lift and drag coefficients. We analyse the open access data, corresponding to 2D experimental testing of a scale prototype LiftWEC cyclorotor conducted by Ecole Centrale Nantes (ECN), using an analytical control-oriented point-vortex model. The current study includes validation of the point vortex model against experimental results, derivation of the lift and drag coefficients for hydrofoils in waves, and analysis of their pre-stall behaviour.

***Index Terms*—Cyclorotor, Model Validation, Wave Energy Converters, LiftWEC, Hydrofoils, Experimental Results**

I. Introduction

Ocean waves are the world's largest untapped source of renewable energy [1]. The Intergovernmental Panel on Climate Change (IPCC) assessed their potential energy production at 29500 TWh per year [2]. Ocean waves also have the highest renewable energy density compared to already developed sources such as wind or solar technologies. However, despite almost 50 years of research and development, no commercially successful wave energy harvesting technology has been developed. None of the traditional wave energy converters (WECs), which use buoyancy or diffraction wave forces, have proven themselves to be commercially viable in terms of the levelised cost of energy (LCoE) [3]. This, along with increasing national and international pressure to reduce dependency on non-renewable sources of energy, creates the motivation to develop new approaches to wave energy conversion. One of the new and most promising concepts is a cyclorotor-based wave energy converter (Fig. 1), which uses hydrofoils to generate lift forces [4], [5]. This lift-force-based technology, which is different to traditional wave energy harvesting methods, has started to attract more and more attention from various researchers and organisations [6]–[10].

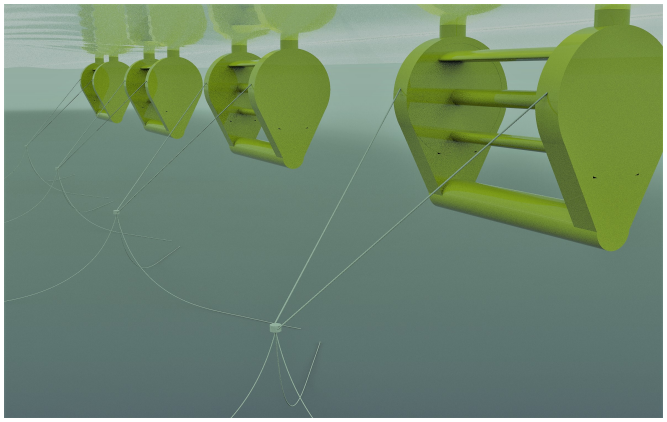

Fig. 1: The LiftWEC cyclorotor-based wave energy converters farm concept, proposed by Gerrit Olbert, TU Hamburg

The proposed wave harvesting method uses the circular motion of water particles caused by wave propagation. Such circulation can generate significant lift forces on the rotating hydrofoils, with optimal cyclorotor control requiring the hydrofoils to follow the direction of water particle circulation, thus maintaining the optimal angle of attack [11]–[14]. The

This project has received funding from the European Union's Horizon 2020 research and innovation programme under grant agreement No. 851885. This work was supported by Science Foundation Ireland under Grant number 20/US/3687. The authors are grateful for the support of the Irish Centre for High-End Computing (ICHEC).

979-8-3503-3226-1/23/$31.00 ©2023 IEEE

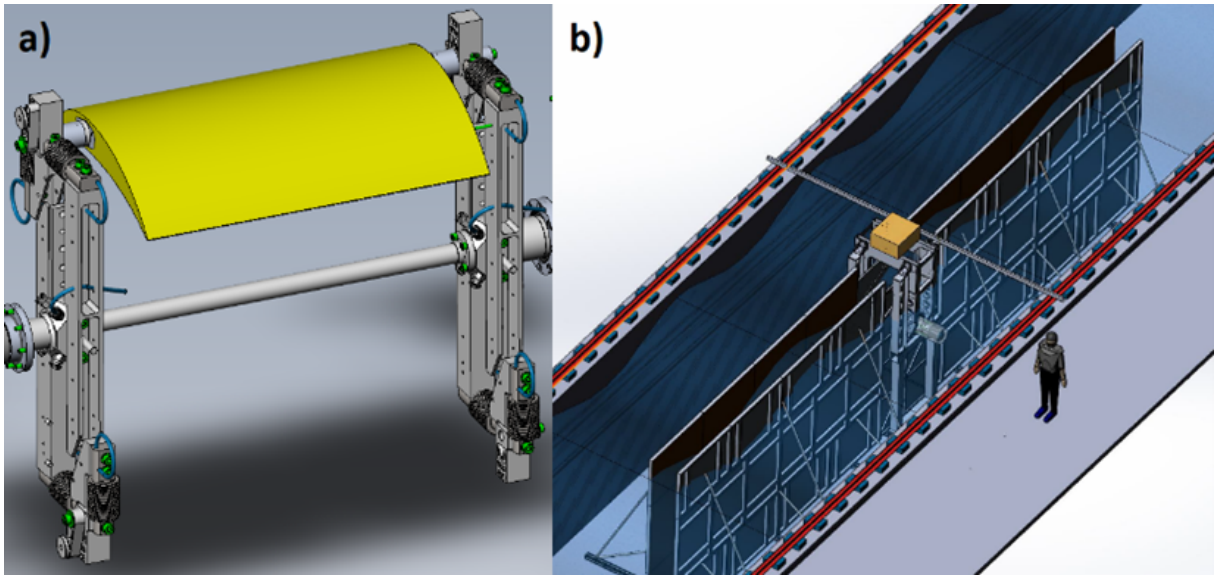

Fig. 2: a) Prototype of a single-foil cyclorotor WEC; b) Experimental setup;

tangential component of the lift force generates a torque on the cyclototor shaft, providing direct (unidirectional) input to the electricity generator.

The most recent performance assessment conducted by the Atargis energy corporation [6], for their cyclorotor concept with two hydrofoils (CycWEC) [15], estimates electricity production at 3000 MW/h for regular, and 1800MW/h for irregular, waves [16]. The CycWEC was also selected as the preferred WEC due to its highest electrical energy production ($\sim 40\%$) and power load factor ($\sim 45\%$) for the Galician coast (NW Spain) in assessments conducted in [17].

A further independent performance assessment was conducted within the LiftWEC consortium [7], estimating an optimistic LCoE for the developed cyclorotor-based LiftWEC concept (Fig. 1) at $\sim$ 140 €/MWh [7]. This competitive cost is justified by the similarity to offshore wind and 'propeller based' technology [18]. The LiftWEC device could also be considered complimentary to offshore wind technology, with possible installation on existing floating platforms.

However, recent [7], [15], [16] and older [19], [20] performance assessments are based on ideal lift and drag coefficients, the values for which were obtained for aerofoils in the ideal conditions of aerodynamic tubes. In this study, we question the equivalence between aerofoils and hydrofoils in waves, in terms of lift and drag coefficients. There is no doubt that influences of the free surface and unsteady lift effects will have a significant effect on the actual lift and drag coefficients values.

In Section II, the authors describe the experimental test of a 2D LiftWEC prototype [21], [22] conducted at École Centrale de Nantes (ECN), France in 2022. Section III is dedicated to the mathematical point-vortex model for single hydrofoil a rotating in waves, documenting equations, assumptions and limitations. In Section IV, the authors derive lift and drag coefficients from the experimental data, and validate a point-vortex model in terms of generation of tangential and radial forces. The Conclusions (Section V) are dedicated to the discussion of the experimental results and applicability of aerofoil lift and drag coefficients for modelling and performance assessment of cyclorotor WECs.

II. Experimental Setup

The 2D LiftWEC prototype was designed, built and tested by Ecole Centrale Nantes (ECN), France (see Fig. 2). The aim of the conducted experiments was not to model a viable WEC prototype, but rather to produce data in a 2D hydrodynamic environment that can be used for the validation of numerical models. The experimental data, drafts and tests documentation are published (open access) on Zenodo [21], [22]. The validation tests presented in this article use the same experiment numbering system as the experimental data sets.

The LiftWEC prototype was tested in the ECN wave and towing tank, in a narrow 'sub-channel' located inside of the overall tank volume (Fig. 2b). Wave gauges were installed inside the sub-channel to measure free surface elevation both up-wave and down-wave of the rotor. Waves were generated by a wave-maker, consisting of a single hinged flap covering the entire width of the tank. Such an experimental setup allows the use of a tank capable of generating large waves, while providing conditions consistent with the narrow width of the device. Unfortunately, the sub-channel setup led to the generation of parasitic waves at the inlet and outlet of the sub-channel (Fig. 2b). While the influence of the waves reflected from the inlet can be ignored, the waves reflected from the outlet cause a significant disturbance to the experimental data. In our validation exercise, we attempt to mitigate such effects by using the parts of the time series data obtained before the waves reflected from outlet reach the cyclorotor.

Fig. 3: Rotor with fairings in a sub-canal (Photo of the experiment)

The tested 2D LiftWEC prototype allows for the installation of one or two curved foils NACA0015, with chord lengths C = 0.3 m, and span S = 0.49 m. The cyclorotor has a radius R = 0.3 m and a submergence depth of the rotor axis at y_0 = -0.755 m. Special circular fairings (Fig. 3) were developed to mask the rotor arms and to provide close to 2D flow conditions in a 'sub-channel'. The rotational velocity of the hydrofoil is controlled using a power take off (PTO) system utilising an electrical motor/generator system, capable of controlling both speed and torque. Installed sensors permit measurement of the PTO torque, radial and tangential forces, and the position of the hydrofoils in polar coordinates (see Fig. 2a). The rotating hydrofoil experienced additional centrifugal force which affected the measured radial and tangential forces values. Such influences were removed in the corrected and published data sets. The measured hydrofoil position coordinates were used for calculation of rotational velocity, introducing additional noise into the experimental data.

III. Analytical Model of the Experimental Tests

The point vortex model, introduced in [23]–[25], proposes a near wake hydrodynamic hydrofoil model and derives a simplified potential for it. The mathematical model of a hydrofoil includes the assumptions of previous researchers [19], [26] and has been validated against their experimental and numerical results, in terms of free surface perturbation caused by hydrofoil rotation. The authors [23] have proposed to consider lift C_L and drag C_D coefficients as 'tuning parameters' in order to account for unmodeled hydrodynamic effects in the control oriented model. Such coefficients can be estimated from CFD simulationS or experimental tests. A trained neural network algorithm could also potentially predict such coefficients.

Another innovation of the point source model is based on the assumption that the lift F_L and drag F_D forces are caused by the fluid/foil interation with an overall relative velocity $\hat{\mathbf{V}}_\mathbf{i}$, which can be evaluated as the vector difference between the wave induced fluid velocity $\mathbf{V}_{\mathbf{W_i}}$ and the hydrofoil rotational velocity $\mathbf{V}_{\mathbf{R_i}}$, plus the influence of waves radiated by the rotating hydrofoil $\mathbf{V}_\mathbf{H}$:

$$\hat{\mathbf{V}}_\mathbf{i} = \mathbf{V}_{\mathbf{W_i}} - \mathbf{V}_{\mathbf{R_i}} + \mathbf{V}_{\mathbf{H_i}} \tag{1}$$

The position (x, y) of a hydrofoil at an instant t, and its instantaneous rotational velocity $\mathbf{V}_\mathbf{R}$, can be found as:

$$x(t) = R\sin(\theta(t)) \tag{2}$$
$$y(t) = y_0 + R\cos(\theta(t)) \tag{3}$$

and

$$V_{Rx}(t) = R\dot{\theta}(t)\cos(\theta(t)) \tag{4}$$
$$V_{Ry}(t) = -R\dot{\theta}(t)\sin(\theta(t)) \tag{5}$$

respectively, where R is the radius of the rotor, y_0 is the submergence depth of the rotor centre, $\theta(t)$ is the polar coordinate of the hydrofoil, and $\dot{\theta}(t)$ is the rotor angular velocity (Fig. 4).

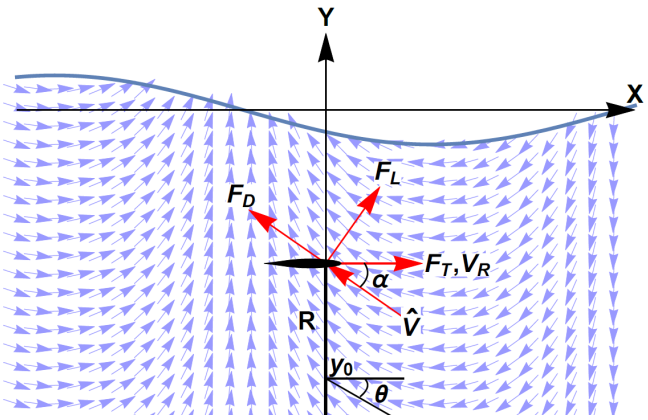

Fig. 4: Force/motion diagram of a hydrofoil, which rotates in waves: θ - polar angle position of the hydrofoil, V_R - the instantaneous rotational velocity of the foil, $\hat{V}$ - the overall relative foil/fluid velocity, α - the attack angle, F_L, F_D, F_T - lift, drag and tangential forces.

In this article, we consider rotation in monochromatic waves,approximated by Airy waves, which have the following potential:

$$\Phi_W = \frac{Hg}{2\omega} e^{ky} \sin(kx - \omega t + \phi) \tag{6}$$

where H is the wave height, g is gravitational acceleration, ω is the wave frequency, k is the wave number, ϕ is the relative phase between the hydrofoil top dead centre position and the wave crest location above the cyclorotor shaft.

The free surface elevation η at a position x, caused by wave propagation, can be found as:

$$\eta = -\frac{1}{g}\left(\frac{\partial \Phi_W}{\partial t}\right)_{y=0} = \frac{H}{2}\cos(kx - \omega t + \phi) \quad (7)$$

The velocity components $\mathbf{V_W}$ of the wave-induced water particle velocity can be found as the gradient of the Airy potential in eq. (6) as:

$$\mathbf{V_W} = \nabla \mathbf{\Phi_W} = \frac{Hgk}{2\omega} e^{ky}\{\sin(kx - \omega t + \phi), \cos(kx - \omega t + \phi)\} \quad (8)$$

The velocity components of the wakes caused by a moving hydrofoil can be found as:

$$\mathbf{V_H} = \frac{\partial \mathcal{F}(\mathbf{z}, \mathbf{t})}{\partial \mathbf{z}} = (\mathbf{V_H})_{\mathbf{x}} - \mathtt{i}(\mathbf{V_H})_{\mathbf{y}} \quad (9)$$

In [23], [24] the simplified complex potential is derived for the point-vortex in the following form:

$$\mathcal{F}(z,t) = \frac{\Gamma(t)}{2\pi \mathtt{i}} Log\left[\frac{z - c(t)}{z - \tilde{c}(t)}\right] - \frac{2\mathtt{i}\sqrt{g}}{\pi}\int_0^t \frac{\Gamma(\tau)}{\sqrt{\mathtt{i}(z - \tilde{c}(\tau))}} D\left[\frac{\sqrt{g}(t-\tau)}{2\sqrt{\mathtt{i}(z - \tilde{c}(\tau))}}\right] d\tau \quad (10)$$

where $z = x + \mathtt{i}y$ is the coordinate in the complex plane, $c(\tau) = x(\tau) + \mathtt{i}y(\tau)$ is the previous position of the foil at dynamic time τ, $\tilde{c}(\tau)$ is the complex conjugate position, and $D(x)$ is the Dawson function [27]:

$$D(x) = e^{-x^2}\int_0^x e^{y^2} dy. \quad (11)$$

It is assumed that the intensity of circulation of the vortex Γ is proportional to the lift force F_L generated on the foil, in accordance with the Kutta-Joukowski theorem [28]:

$$\Gamma = F_L/(\rho|\hat{V}|) = \frac{1}{2} C_L(\alpha)\,|\hat{V}|\,C \quad (12)$$

where ρ is the fluid density, $C_L(\alpha)$ the lift coefficient, which is a function of the angle of attack α, and C the length of the hydrofoil chord.

Then, the near wake field $\mathbf{V_H}$, caused by foil rotation for the case of a single hydrofoil, can be evaluated using only the integral part of equation (10). The inclusion of the near fluid velocity field permits correction of the estimate of the angle of attack for the rotor foil:

$$\alpha(t) = \arcsin\left(\frac{(V_R)_x * (\hat{V})_y - (V_R)_y * (\hat{V})_x}{|V_R||\hat{V}|}\right) + \gamma \quad (13)$$

where γ is a hydrofoil pitch angle.

The lift F_L and drag F_D forces generated on the hydrofoil can be calculated using the following equations:

$$F_L = \frac{1}{2}\rho\, C\, S\, C_L(\alpha)\,|\hat{V}|^2 \quad (14)$$

$$F_D = \frac{1}{2}\rho\, C\, S\, C_D(\alpha)\,|\hat{V}|^2, \quad (15)$$

where C is the chord length, S is the span of the hydrofoil, $\hat{V}$ is the relative foil/fluid velocity, and C_L and C_D are lift and drag coefficients, respectively.

Then, the tangential F_T and radial F_R forces can be found as:

$$F_T = F_L\,\sin(\alpha - \gamma) - F_D\,\cos(\alpha - \gamma) \quad (16)$$

$$F_R = F_L\,\cos(\alpha - \gamma) + F_D\,\sin(\alpha - \gamma). \quad (17)$$

Validation of the models in terms of tangential F_T and radial F_R forces is a focus of the LiftWEC project [29]–[31]. The benefit of using these metrics is that it allows the evaluation of lift C_L and drag C_D coefficients, which are important for estimation of the power which could be generated by a full-scale device.

The proposed control-oriented point-vortex model [23] has been successfully validated against CFD simulation in [32], for attached flow conditions. However, the model can underestimate loads for large angles of attack, due to unsteady lift effects.

IV. Validation Results

A. Selection and preparation of the data-sets for analysis

Fig. 5 illustrates the selection of the best time interval for analysis for Test number 109. The selection is based on the free surface elevation up-wave, down-wave, and corresponding changes in the angular velocity and radial force. In the presented experiment, a single hydrofoil with pitch $\gamma = 0^o$ rotates in a regular wave H=0.2m, T=1.6s, with phase $\phi = 90^o$. The free surface elevation data from 'Gauge 4', located 1 metre up-wave from the cyclorotor, and 'Gauge 6', located 1 metre down-wave from the cycorotor, are used for modelling the incident and transmitted waves.

The blue lines in Fig. 5 correspond to the measured data while the red line is the analytical Airy wave (7) approximation of the free surface elevation caused by the incident (a) and transmitted (b) waves. The time interval shows only the development of the incoming wave from 41 to 51 s in Fig. 5, and cannot be used for analysis. The time frame from 57 to 67 s in Fig. 5b illustrates the influence of the reflected waves, which cause significant fluctuation of the radial force (Fig. 5c). As a result, only the short time window from 51 to 57 seconds can be used for experimental data analysis. The selected time interval shows the reasonable fluctuation of the radial force, in Fig. 5c, and wave cancellation effects, in Fig. 5a,b.

The measured loading from the installed coupled sensors (see Fig. 2) can be converted to a two-dimensional model by summation of two measurements, and subsequent division by the foil span S:

$$F_{T_{2D}} = (F_{T_{cell_1}} + F_{T_{cell_2}})/S \quad (18)$$

$$F_{R_{2D}} = (F_{R_{cell_1}} + F_{R_{cell_2}})/S \quad (19)$$

The direction of forces and the measured half-chord position provided from the experimental data are not in agreement with the point vortex oriented coordinate system, due to the vortex location. Therefore, a 14.5^o shift correction is applied, and focus on the location of the point vortex on the hydrofoils quarter chord [29]:

$$\tilde{F}_T = F_{T_{2D}} \cos(14.5^o) - F_{R_{2D}} \sin(14.5^o) \quad (20)$$

$$\tilde{F}_R = F_{T_{2D}} \sin(14.5^o) + F_{R_{2D}} \cos(14.5^o) \quad (21)$$

$$\theta_{2D} = \theta + 14.5^o \quad (22)$$

The shifted and corrected values of the tangential F_T and radial F_R force are used in the analytical point vortex model for estimation of the lift C_L and drag C_D coefficients using enqs. (16) and (17).

B. Analysis and validation of the selected cases

Fig. 6a,b illustrates the lift and drag coefficients derived for Test 109,for which the time interval for analysis is defined in Fig. 5. In Test 109, a hydrofoil with the zero pitch angle $\gamma = 0$ is rotated in monochromatic waves with H=0.2m and T=1.6s, with angular velocity equal to the wave frequency $\dot{\theta} = \omega$, and relative phase $\phi = 90^o$. The horizontal axis in Fig. 6a,b represents the position of the foil (in degrees) where 0^o corresponds to the foil at top dead centre. The left vertical axis of Fig. 6a,b corresponds to the experimentally measured lift coefficient values (blue points), and their trend (red line), while the right vertical axis corresponds to the estimated angles of attack for different foil positions (black line). The hydrofoil, during Test 109, experiences small angles of attack from -2 to -7 degrees, and operates under a Reynolds number between 257,000 and 292,000. Figs. 6a,b show that the obtained lift coefficients are more sensitive to the position of the foil and direction of its rotation than the angle of attack, while the drag coefficients are more sensitive to angle of attack than submergence depth. The maximum identified lift coefficient $C_L = 0.35$ corresponds to foil position of $\theta = 140^o$ and small angle of attack $\alpha = -3^o$. The obtained lift coefficient value is comparable with the corresponding lift coefficient for an airfoil, at $C_L = 0.33$. However, the lift coefficient is significantly underestimated for larger angles of attack, with an expectation to reach C_L =0.739 for $\alpha = -7^o$ [33]. The representation of the lift and drag coefficients as functions of the angle of attack and position of the foil allow the best validation with the experimental results to be achieved in terms of generation of tangential and radial forces 6c,d.

The second validation example considers larger values of angle of attack that the foil experienced during Test 110 (see Fig. 7). In Test 110, a hydrofoil with a zero pitch angle $\gamma = 0$ is rotated in monochromatic waves with H=0.253m and T=1.8s, with an angular velocity consistent with the wave frequency $\dot{\theta} = \omega$, and non-ideal relative phase $\phi = 80^o$. The lift coefficient achieves a maximum value of $C_L = 0.9$ for $\alpha = -8^o$ at position $\theta = 80^o$. The average estimated lift coefficient value $C_L = 0.7$ is in agreement with the average lift coefficient value for an airfoil, which is $C_L = 0.75$ [33]. However, the hydrofoil experiences more significant drag, at $C_D = 0.12$ for $\alpha = -8^o$. Such a value is much greater than the drag coefficient obtained for airfoil, at $C_D \approx 0.02$. The development of dedicated optimal hydrofoils (rather than using existing aerofoil shapes) for a cyclorotor could potentially solve this problem.

Fig. 8a,b illustrates the lift and drag coefficients derived for Test number 112. Test 112 is selected because, for this case, hydrofoil NACA0015 operates in the vicinity of the stall angle $\alpha_{stall} = 15^o$, for which the maximum power is generated in simulations conducted in [15]. In Test 112, a hydrofoil with zero pitch angle $\gamma = 0$ is rotated in monochromatic waves with H=0.31m and T=2s, with an angular velocity consistent with the wave frequency $\dot{\theta} = \omega$, and relative phase $\phi = 90^o$. The lift and drag coefficients are obtained for the time interval from 40.25 to 47.25 s, which is relatively clear of wave reflections.

Fig. 8a shows that the lift coefficient achieves its extremum twice over the plotted period, when $\alpha = -12^o$, with maximum lift occurring when the hydrofoil moves towards its lowest point in the cycle ($\theta = 70^o, C_L = 1.15$), but with a weaker response when the foil approaches the free surface ($\theta = 250^o, C_L = 0.8$). Such a difference can be explained by the unsteady hydrodynamics of hydrofoils, specifically flow separation and deep dynamic stall effects [34]–[36]. Such effects can significantly decrease the realistic potential performance of a cyclorotor. The estimated range of the lift coefficient C_L from ≈ 0.8 to 1.2 for $\alpha = -12^o$, for experimental Reynolds number of approximately from 100,000 to 400,000, is in broad agreement with the lift coefficient $C_L = 0.9285$ obtained in [33] for an aerofoil for a Reynolds number $Re = 360,000$. However, the hydrofoil also experiences significantly greater drag, of $C_D \approx 0.225$, while $C_D = 0.123$ is the maximum for an aerofoil with a similar angle of attack. However, this difference is not particularly significant, as identified in Test 109. The lift and drag coefficients determined within the assumptions of the model depend not only on the angle of attack and Reynolds number, but also on the position of the foil and the direction of movement. This representation of the coefficients allows faithful reproduction of the experimental measurements of radial and tangential forces. Fig. 8c,d illustrates good validation against experimentally measured tangential and radial forces, after implementation of the proposed representation.

Clearly, the values of lift and drag coefficients determined from the experimental data may be influenced by hydrodynamic and mechanical effects which are not accounted for in the parametric structure of the point-vortex model. However, given the relatively close agreement between the lift and drag coefficients evaluated from the experimental data for hydrofoils, and the coefficients experimentally estimated for airfoil NACA0015 [33], it appears that the parametric structure of the model is relatively sound. Validation and analysis of the experimental tests of deep stall effects,for rotation of a single hydrofoil in still water, and two hydrofoils in waves, can be found in [37].

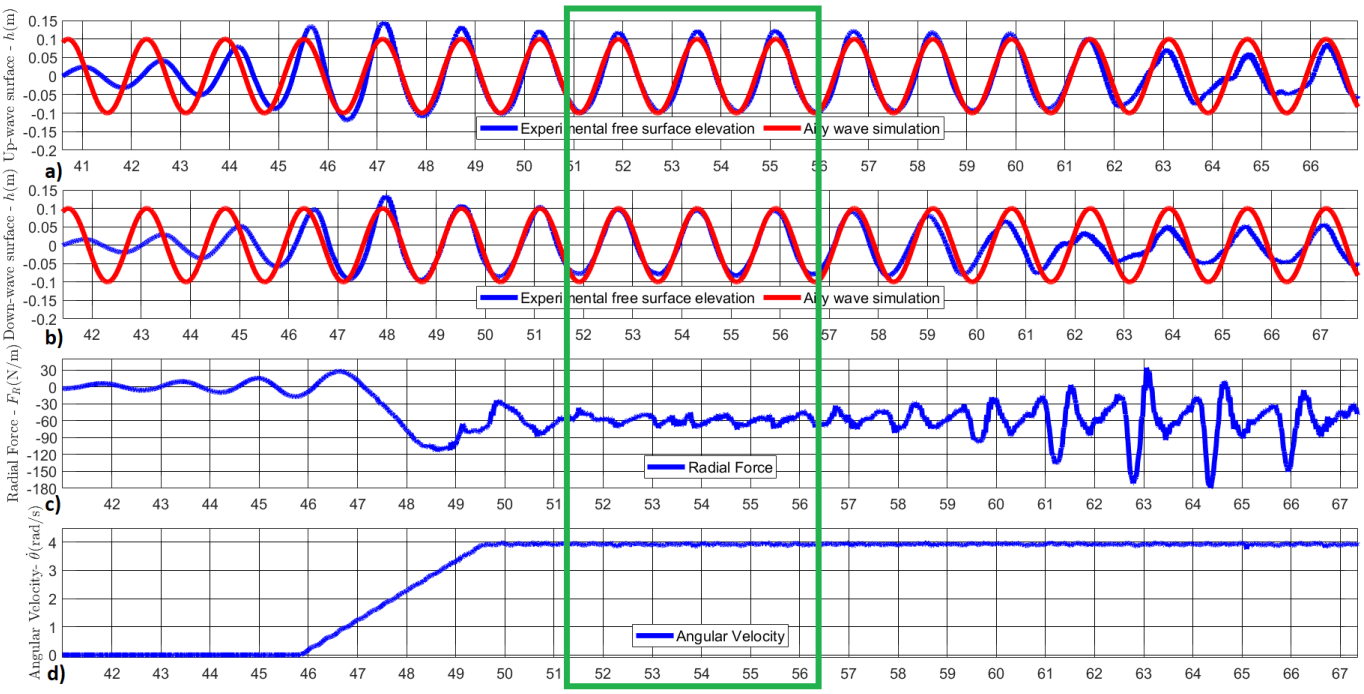

Fig. 5: Determination of the time-frame for experimental data analysis, Test 109. In Test 109 a single hydrofoil with pitch $\gamma = 0^o$ rotates in regular wave H=0.2m, T=1.6s and relative phase $\phi = 90^o$.

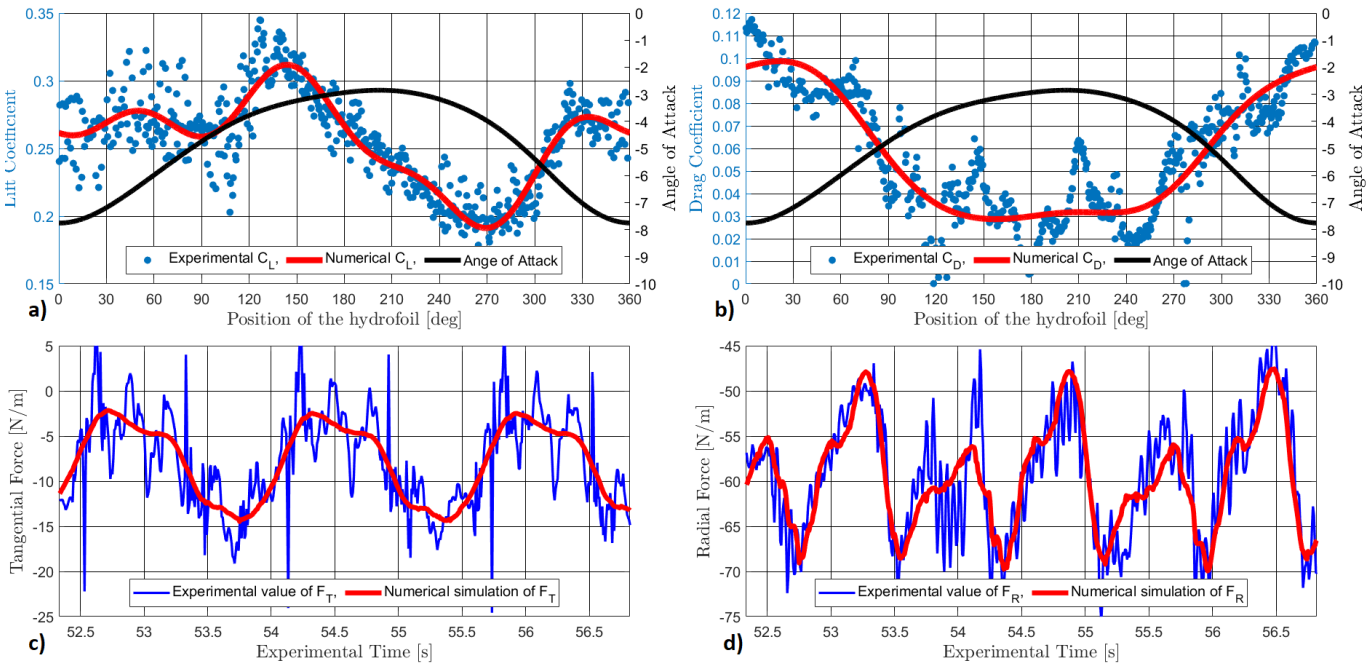

Fig. 6: Derivation of the lift and drag coefficients (a,b) and their validation against experimental data (c,d) for Test 109. In Test 109, a hydrofoil with zero pitch angle $\gamma = 0$ was rotated in monochromatic wave H=0.2m and T=1.6s, with the wave frequency $\dot{\theta} = \omega$ and relative phase $\phi = 90^o$.

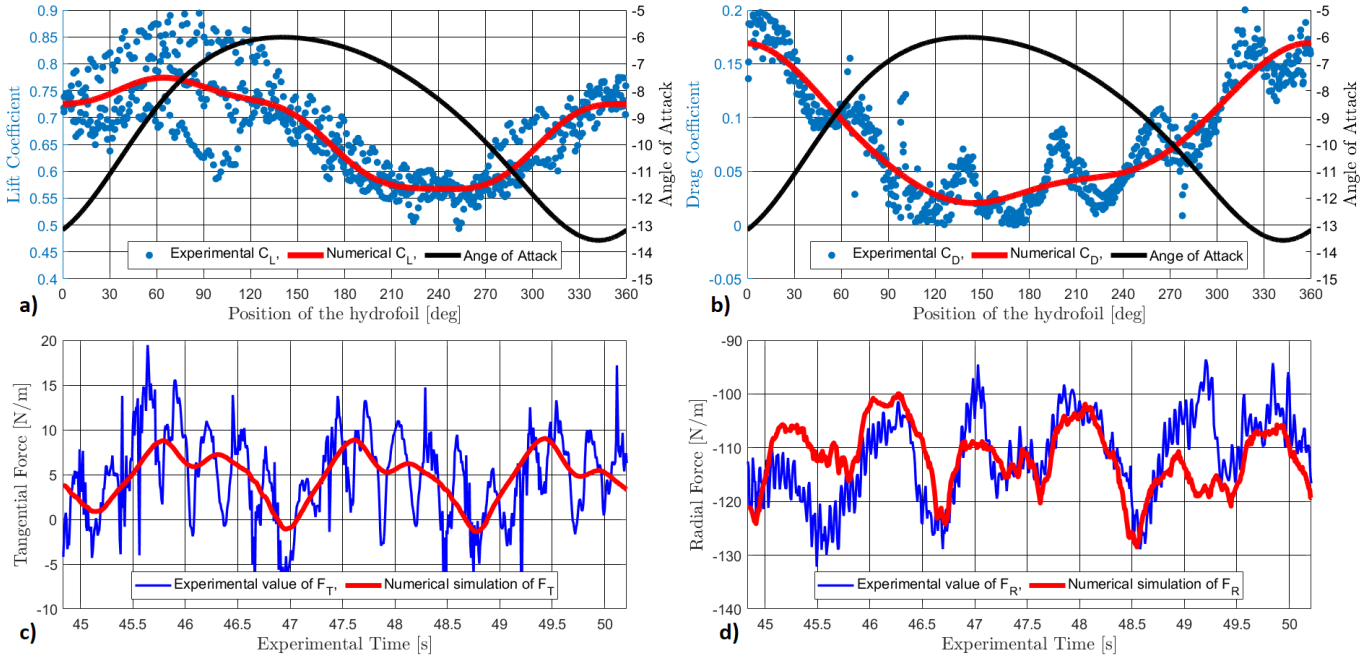

Fig. 7: Derivation of the lift and drag coefficients (a,b) and their validation against experimental data (c,d) for Test 110. In Test 110, a hydrofoil with zero pitch angle $\gamma = 0$ was rotated in monochromatic wave H=0.253m and T=1.8s, with the wave frequency $\dot{\theta} = \omega$ and relative phase $\phi = 80^o$.

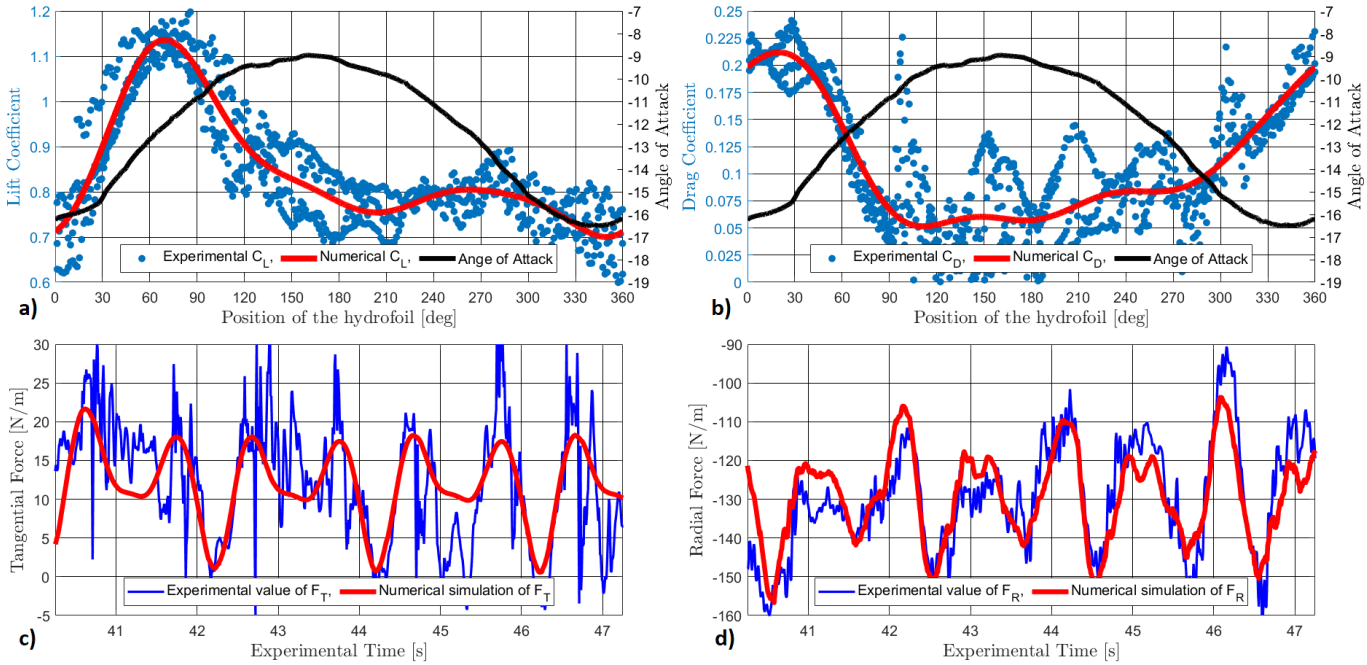

Fig. 8: Derivation of the lift and drag coefficients (a,b) and their validation against experimental data (c,d) for Test 112. In Test 112, a hydrofoil with zero pitch angle $\gamma = 0$ was rotated in monochromatic wave H=0.31m and T=2s, with wave frequency $\dot{\theta} = \omega$ and relative phase $\phi = 90^o$.

V. Conclusion

The presented experimental data and model validation are limited to the 2D monochromatic wave cases. Nevertheless, the obtained values of lift and drag coefficients are realistic and comparable with the lift and drag coefficients obtained for aerofoils [33]. It gives us some level of confidence in the lift and drag coefficients for the much larger Reynolds number, used within research dedicated to the full-scale device performance predictions [15], [16], [37], [38]. However, due to the significant influences of the free surface and unsteady effects, the lift and drag coefficients should be considered not only as functions of the angle of attack and Reynolds number but also the position of the foil and the direction of its movement. Ideally, such coefficients could be predicted using a machine learning method, trained on experimental test data or hi-fidelity CFD simulation. These coefficients can then be used for the development of optimal control strategies for more complex panchromatic sea states, using methods developed in [11], [13], [14].

In general, validation of the model against experimental results is successful and the authors recommend the point vortex model for further control design and performance assessment studies. Certainly, the model does not consider complex nonlinear wave/foil hydrodynamic interaction effects, nor influences of the free surface or the potential generation of evanescent modes in the vicinity of the cyclorotor. However, such simplifications facilitate a significantly decrease in the model computation time, making the model suitable for real-time control calculations. Efficient application of the point-vortex model for real-time control will require further linearisation and optimisations of the model, estimator development for the cyclorotor state, and predictors for relative foil/fluid velocity.

Analysis of the experimental results has identified new challenges for cyclorotor WEC technology, such as requirements for further optimisation of the hydrofoil profile, in order to maintain attached flow and avoid the flow separation. The experimental hydrofoils NACA0015, operating under Reynolds number from approximately 100,000 to 400,000 were not able to maintain attached flow for relatively large angles of attack. This can be explained by the fact that, for foils NACA0015, it is difficult to maintain attached flow, even under optimal conditions in very clean wind tunnels. Thus, it is important to develop specialised foils dedicated to rotation in wave conditions. New foil designs could also potentially reduce drag losses.

Nevertheless, the conducted analysis of the experimental data confirms that the generation of lift force and estimated lift coefficients are comparable with values measured for airfoils. It creates motivation for further development of the cyclorotor based wave energy converters.

References

[1] J. V. Ringwood, G. Bacelli, and F. Fusco, "Energy-maximizing control of wave-energy converters: The development of control system technology to optimize their operation," *IEEE Control Systems Magazine*, vol. 34, no. 5, pp. 30–55, 2014.

[2] The Intergovernmental Panel on Climate Change (IPCC), "Renewable Energy Sources and Climate Change Mitigation," https://www.ipcc.ch/report/renewable-energy-sources-and-climate-change-mitigation/ [Accessed: 5-March-2023].

[3] B. Guo and J. V. Ringwood, "A review of wave energy technology from a research and commercial perspective," *IET Renewable Power Generation*, vol. 15, no. 14, pp. 3065–3090, 2021.

[4] M. Folley and T. Whittaker, "Lift-based wave energy converters – an analysis of their potential," in *Proceedings of the 13th European Wave and Tidal Energy Conference, Napoli, Italy*, 2019.

[5] A. Ermakov and J. V. Ringwood, "Rotors for wave energy conversion—practice and possibilities," *IET Renewable Power Generation*, vol. 15, p. 3091–3108, 2021.

[6] Atargis, the Energy Corporation, Available: https://atargis.com// [Accessed: 5-March-2023], 2023.

[7] LiftWEC Consortium, https://liftwec.com/ [Accessed: 5-March-2023], 2023.

[8] C. Yu, L. Andong, Y. Xiaochuan, L. Ziyan, T. Xiaobo, and W. Shiming, "Experimental tests and CFD simulations of a horizontal wave flow turbine under the joint waves and currents," *Ocean Engineering*, vol. 237, p. 109480, 2021.

[9] X. Wu and L. Zuo, "Preliminary modeling of angle of attack in self-rectifying turbine under high rotational speed," in *Proceedings of the ASME: the 34th Conference on Mechanical Vibration and Sound (VIB)*, 2022.

[10] Z. Yin and M. Esmaeilpour, "The hydrodynamic performance of a turbine in shallow free surface flow," *J Hydrodyn*, vol. 33, p. 804–820, 2021.

[11] A. Ermakov, A. Marie, and J. V. Ringwood, "Optimal control of pitch and rotational velocity for a cyclorotor wave energy device," *IEEE Transactions on Sustainable Energy*, vol. 13, no. 3, pp. 1631–1640, 2022.

[12] A. M. Ermakov, A. Marie, and J. V. Ringwood, "Some fundamental results for cyclorotor wave energy converters for optimum power capture," *IEEE Transactions on Sustainable Energy*, vol. 13, no. 3, pp. 1869–1872, 2022.

[13] J. V. Ringwood and A. Ermakov, "Energy-maximising control philosophy for a cyclorotor wave energy device," in *41st International Conference on Ocean, Offshore & Arctic Engineering (OMAE), Hamburg*, no. 80990. American Society of Mechanical Engineers, 2022.

[14] A. Arredondo-Galeana, A. Ermakov, W. Shi, J. V. Ringwood, and F. Brennan, "Control strategies for power enhancement and fatigue damage mitigation of wave cycloidal rotors," Available: https://papers.ssrn.com/sol3/papers.cfm?abstract_id=4346306 [Accessed: 5-March-2023], 2023.

[15] S. G. Siegel, "Numerical benchmarking study of a cycloidal wave energy converter," *Renewable Energy*, vol. 134, pp. 390–405, 2019.

[16] K. C. Chitale, C. Fagley, A. Mohtat, and S. G. Siegel, "Numerical evaluation of climate scatter performance of a cycloidal wave energy converter," *International Marine Energy Journal*, vol. 5 (3), pp. 315—-326, 2022.

[17] B. Arguilé-Pérez, A. S. Ribeiro, X. Costoya, M. De-Castro, P. Carracedo, J. M. Dias, L. Rusu, and M. Gómez-Gesteira, "Harnessing of different WECs to harvest wave energy along the Galician coast (NW Spain)," *Journal of Marine Science and Engineering*, vol. 10, no. 6, 2022.

[18] A. Martinez and G. Iglesias, "Mapping of the levelised cost of energy for floating offshore wind in the European Atlantic," *Renewable and Sustainable Energy Reviews*, vol. 154, p. 111889, 2022.

[19] A. Hermans, E. Van Sabben, and J. Pinkster, "A device to extract energy from water waves," *Applied Ocean Research*, vol. 12, no. 4, pp. 175–179, 1990.

[20] N. Scharmann, "Ocean energy conversion systems: the wave hydro-mechanical rotary energy converter," Ph.D. dissertation, PhD Thesis, Institute of Mechanics and Ocean Engineering, TUHH, Hamburg, Germany, 2018.

[21] F. Thiebaut, G. Payne, S. Haquin, M. Weber, S. Lamber, and B. Pettinotti, "LiftWEC project deliverable D4.3 Open access experimental

data from 2D scale model," https://doi.org/10.5281/zenodo.5534471 [Accessed: 5-March-2023], 2021.
[22] F. Thiebaut and G. Payne, "LiftWEC project deliverable D4.4 Report on Physical Modelling of 2D LiftWEC Concepts," https://cordis.europa.eu/project/id/851885. [Accessed: 5-March-2023], 2021.
[23] A. Ermakov and J. V. Ringwood, "A control-orientated analytical model for a cyclorotor wave energy device with N hydrofoils," *Journal of Ocean Engineering and Marine Energy*, vol. 7, pp. 201–210, 2021.
[24] A. M. Ermakov and J. V. Ringwood, "Erratum to: A control-orientated analytical model for a cyclorotor wave energy device with N hydrofoils," *Journal of Ocean Engineering and Marine Energy*, vol. 7, p. 493–494, 2021.
[25] A. Ermakov and J. V. Ringwood, "Development of an analytical model for a cyclorotor wave energy device," in *Proceedings of 14th European Wave and Tidal Energy Conference, paper #1885, Plymouth, UK*, 2021.
[26] C. P. Fagley, J. J. Seidel, and S. G. Siegel, "Wave cancellation experiments using a 1:10 scale cycloidal wave energy converter," in *Proceedings of 1st Asian wave and Tidal Conference Series,Jeju Island, Korea*, 2012.
[27] H. G. Dawson, "On the numerical value of $\int_0^h e^{x^2}\,dx$," *Proceedings of the London Mathematical Society*, vol. s1-29 (1), pp. 519–522, 1897.
[28] G. K. Batchelor, *An Introduction to Fluid Dynamics*. Cambridge University Press, 1967.
[29] G. Olbert, L. Papillon, R. Pascal, A. Ermakov, and F. Thibaut, "LiftWEC project deliverable D3.3: Tool validation and extension report," https://cordis.europa.eu/project/id/851885 [Accessed: 5-March-2023], 2021.
[30] A. Ermakov, J. V. Ringwood, G. Olbert, A. Arredondo-Galeana, R. Pascal, L. Papillon, F. Thiebaut, and P. Grégory, "LiftWEC project deliverable D5.2 Validated numerical model with real-time computational capabilities," https://cordis.europa.eu/project/id/851885 [Accessed: 5-March-2023], 2021.
[31] A. Ermakov and J. V. Ringwood, "A validated analytical model for a cyclorotor wave energy device," *International Marine Energy Journal*, vol. 5, no. 2, p. 201–208, 2022.
[32] A. Arredondo-Galeana, G. Olbert, W. Shi, and F. Brennan, "Near wake hydrodynamics and structural design of a single foil cycloidal rotor in regular waves," *Renewable Energy*, vol. 206, pp. 1020–1035, 2023.
[33] R. Sheldahl and P. Klimas, *Aerodynamic characteristics of seven symmetrical airfoil sections through 180-degree angle of attack for use in aerodynamic analysis of vertical axis wind turbines*. Sandia National Labs., Albuquerque, 1981.
[34] T. Gabriel and M. Ignazio, "Unsteady hydrodynamics of tidal turbine blades," *Renewable Energy*, vol. 146, pp. 843–855, 2020.
[35] L. Shi, A.-C. Bayeul-Lainé, and O. Coutier-Delgosha, "Numerical investigations on unsteady vortical flows and separation-induced transition over a cycloidal rotor at low reynolds number," *Energy Conversion and Management*, vol. 266, p. 115812, 2022.
[36] L. Shi, A.-C. Bayeul-Laine, and O. Coutier-Delgosha, "Analysis of flow-induced performance change of cycloidal rotors: Influence of pitching kinematic and chord-to-radius ratio," *Ocean Engineering*, vol. 263, p. 112382, 2022.
[37] A. Ermakov, F. Thiebaut, G. S. Payne, and J. V. Ringwood, "Validation of a control-oriented point vortex model for a cyclorotor-based wave energy device," *Journal of Fluids and Structures*, vol. 119, 2023.
[38] J. Fernandez Chozas, A. Têtu, and A. Arredondo-Galeana, "A parametric cost model for the initial techno-economic assessment of lift-force based wave energy converters," in *Proceedings of 14th European Wave and Tidal Energy Conference, Plymouth, UK*, 2021.